Prognostic Signature: Papillary Thyroid Carcinoma With Poor Prognosis Has Enhanced Immune Escape Capacity And High Tumor Heterogeneity

Xinyang Li
The First Affiliated Hospital of China Medical University: The First Hospital of China Medical University
Zhenyu Xie
The First Affiliated Hospital of China Medical University: The First Hospital of China Medical University
Yinde Huang
The First Affiliated Hospital of China Medical University: The First Hospital of China Medical University
Xin Li
The First Affiliated Hospital of China Medical University: The First Hospital of China Medical University
Yuzhen He
The First Affiliated Hospital of China Medical University: The First Hospital of China Medical University
Song Wu
The First Affiliated Hospital of China Medical University: The First Hospital of China Medical University
Shiyue Wang
The First Affiliated Hospital of China Medical University: The First Hospital of China Medical University
Wenbin Chen
The First Affiliated Hospital of China Medical University: The First Hospital of China Medical University
Yuchen He
The First Affiliated Hospital of China Medical University: The First Hospital of China Medical University
Jian Zhang (jianzhang@cmu.edu.cn)
China Medical University https://orcid.org/0000-0003-4448-0774

Research Article

Keywords: tumor immune microenvironment, prognostic model, papillary thyroid carcinoma, tumor mutation burden, cancer stem cell, tumor heterogeneity, immune escape

Posted Date: May 27th, 2022

DOI: https://doi.org/10.21203/rs.3.rs-1632049/v1

Abstract

Background

Papillary thyroid carcinoma (PTC) is considered an inflammation-driven cancer. However, a systematic investigation of the relationship between the tumor immune microenvironment and the prognosis of PTC has not been conducted.

Methods

A prognostic model based on differentially expressed genes (DEGs) and progression-free survival (PFS) data from The Cancer Genome Atlas (TCGA) was established by least absolute shrinkage and selection operator (LASSO) and multivariate Cox analyses. In total, 502 PTC cases were divided into low prognostic risk score (PR) (L-PR) and high PR (H-PR) groups according to the median PR. We then compared the immune characteristics between groups and verified these differences in five validation cohorts (GSE33630, GSE60542, GSE58545, GSE5364, and GSE27155). Furthermore, we explored cancer stem cells (CSCs) and the tumor mutation burden (TMB) to explain the prognostic results.

Results

A prognostic signature (PR) based on 13 DEGs performed well in prognostic prediction (5-year area under the curve (AUC) = 0.861). The PR was positively correlated with age, stage, T classification, metastasis, *RAS* mutation, and subtypes (follicular or tall cell PTC). Importantly, the H-PR group, which had poor prognostic features, exhibited four main characteristics: comprehensive weakening of the immune system that was not observed in the L-PR group, a higher ratio of tumor-promoting immune cells, more CSCs, and a higher TMB than the L-PR group. Gene set enrichment analysis (GSEA) results also showed the enrichment of immune-related pathways in the L-PR group.

Conclusions

Our prognostic model can effectively predict the prognosis and revealed that immune escape and tumor heterogeneity in the tumor microenvironment (TME) could be mechanisms of poor prognosis in PTC.

1 Introduction

Thyroid cancer (TC), which accounts for 90% of endocrine malignancies and 70% of endocrine cancer deaths (1), is the fifth most common cancer among American women, and the incidence of TC is increasing (2). Papillary thyroid carcinoma (PTC) is a differentiated thyroid carcinoma (DTC) accounting for approximately 84% of TC cases (3). In most patients, standard treatment (surgery + radioactive iodine) has an excellent overall prognosis. While the 5-year survival rate of patients with iodine-sensitive DTC is

approximately 98%, a small proportion (< 10%) of DTC cases cannot be cured by standard therapies and are classified as "advanced thyroid cancer" (4, 5). The recurrence and metastasis of these locally advanced PTCs hinder the survival and clinical management in certain patients. Current treatment strategies for these cancers are inadequate. Using novel and sensitive biomarkers to effectively identify specific patients and provide personalized treatment has become an important research topic.

Inflammatory cells in the tumor microenvironment (TME) show conflicting activities; various proportions of tumor-antagonizing and tumor-promoting immune cells coexist in tumor lesions and can be traced to sites of both chronic inflammation and tumor formation (6). As the largest endocrine organ in the human body, the thyroid gland is a common target for autoimmune diseases (7). Inflammatory cells are widely distributed in the PTC microenvironment. Based on TME immune subgroup, PTC is classified into "inflammatory" tumors (8). A considerable number of previous studies have reported the role of immune cells in TC. Among them, B cells, CD8 + T cells, M1 macrophages, T helper 1 (TH1) cells, natural killer (NK) cells, myeloid dendritic cells (mDCs), and γδ T cells have antitumor effects, while T regulatory cells (Tregs), T helper 2 (TH2) cells, M2 macrophages, myeloid-derived suppressor cells (MDSCs), immature dendritic cells (iDCs), mast cells, monocytes, and neutrophils have tumor-promoting effects (9–11). However, the roles of immune cells in PTC have not been fully elucidated, and their molecular mechanism and causal link with PTC remain unclear. A systematic investigation of the relationship between the tumor immune microenvironment and prognosis in PTC has not been carried out.

Immunotherapy, which strengthens the human immune system to fight tumors, has developed rapidly in recent decades and become the main driving force for personalized medicine. Different immunotherapies targeting TC in which tumor-associated macrophages (TAMs), dendritic cells (DCs), and T cells are targeted to resist tumors are in the trial stage (4). Immunotherapies, especially immune checkpoint inhibitors, are expected to serve as new alternative treatment options for PTC patients with poor prognosis, as their targeting of *CTLA-4, PD-1*, *TIM-3*, *Lag-3*, and *TIGIT* and their ligands can release the immune system and activate cytotoxic lymphocytes (CTLs) to kill TC cells (4). Additionally, the use of tumor mutation burden (TMB) as a biomarker of the response to immune checkpoint blockade has gradually been revealed to have important prognostic value in immunotherapy (12–15). Immunotherapy is more efficacious in tumors with a high TMB, and TMB was added to the 2019 NCCN guidelines for non-small cell lung cancer. However, the report on the role of TMB in PTC has not been carried out. Exploring the relationship between the TMB and PTC may help to screen populations for effective immunotherapy. A further understanding of the molecular and immunological characteristics of the TME will provide novel and more effective immunotherapy strategies for PTC.

Our goal in this study was to understand the characteristics of the inflammatory TME in the prognostic stratification of patients with PTC and to explore more possibilities for PTC treatment. Based on clinical information, we systematically analyzed the expression and prognostic correlation of DEGs and developed a personalized prognostic marker (prognostic risk score, PR) for PTC patients. Bioinformatics analysis was performed to explore immunological interpretations of differences in prognosis at the TME, cellular and molecular levels (Fig. 1). The results of this study can serve as a reference for subsequent

immune-related research and are expected to facilitate screening of suitable populations for PTC immunotherapy.

2 Materials And Methods

2.1 Materials

A thyroid carcinoma (THCA) dataset from The Cancer Genome Atlas (TCGA) with 58 normal thyroid samples (N) and 512 PTC samples (T) was selected as the discovery cohort. Normalized level-three RNA-seq fragments per kilobase of exon per million fragments mapped (FPKM) data and simple nucleotide variation data (VarScan) were downloaded from the TCGA Genomics Data Commons (GDC) (https://portal.gdc.cancer.gov/). Clinical THCA TCGA data were downloaded from the University of California at Santa Cruz (UCSC) Xena platform (https://xena.ucsc.edu/).

The following 7 PTC gene expression microarray datasets were downloaded from the National Center for Biotechnology Information Gene Expression Omnibus (GEO) database (http://www.ncbi.nlm.nih.gov/geo): GSE33630 (N = 45, T = 49), GSE60542 (N = 30, T = 33), GSE58545 (N = 18, T = 27), GSE3467 (N = 9, T = 9), GSE3678 (N = 7, T = 7), GSE5364 (T = 35), and GSE27155 (T = 51).

2.2 Screening of differentially expressed genes (DEGs)

DEGs between PTC and normal thyroid tissues in the TCGA dataset were determined with the “limma” package and the Wilcoxon test in R (adjusted p-value < 0.05 and $|\log_2 FC|>1$).

GEO2R (http://www.ncbi.nlm.nih.gov/geo/geo2r/) was applied to screen GEO datasets (GSE33630, GSE60542, GSE58545, GSE3467, and GSE3678) for DEGs.

2.3 Functional enrichment analysis

To efficiently use DEG data, DEGs that satisfied the following criteria were selected for Gene Ontology (GO) and Kyoto Encyclopedia of Genes and Genomes (KEGG) enrichment analyses (DAVID 6.7, https://david-d.ncifcrf.gov/):

- 1 differential expression in the TCGA dataset and
- 2 differential expression in at least 4 of the 5 GEO datasets.

2.4 Construction of a prognostic model

We defined common DEGs from comparisons of the TCGA data and the five GEO datasets as verified differentially expressed genes (VDEGs); these VDEGs were then subjected to least absolute shrinkage and selection operator (LASSO) analysis (16). Modeling genes with the best λ values, which were screened by 1000-fold cross-validation, were determined. Multivariate Cox analysis of the modeling genes and

progression-free survival (PFS) were used to generate prognostic risk scores (PRs) with the following equation:

PR=$\sum$ (mRNA expression * regression coefficient β).

A total of 502 TCGA cases were divided into low PR (L-PR) and high PR (H-PR) groups based on the median PR. To validate the reliability of the modeling genes, univariate Cox regression analysis was used to verify the association of each modeling gene with the prognosis.

2.5 Comparison of the tumor immune microenvironment in the L-PR and H-PR groups

2.5.1 ESTIMATE

ESTIMATE was used to evaluate the level of immune cell infiltration (immune score), stromal content (stromal score), stromal-immune comprehensive score (ESTIMATE score) and tumor purity for each THCA sample (17).

2.5.2 Expression-based stemness index (mRNAsi)

The mRNAsi levels of the THCA data were used to measure the cancer stem cell (CSC) content (18). mRNAsi levels were evaluated with a predictive model using one-class logistic regression (OCLR). We downloaded mRNAsi data from https://gdc.cancer.gov/about-data/publications/PanCanStemness-2018.

2.5.3 TIMER

The TIMER online database was used to analyze and visualize the abundance of 6 subtypes of tumor-infiltrating immune cells (B cells, CD4 + T cells, CD8 + T cells, macrophages, neutrophils, and DCs) (19). We downloaded data on immune infiltration in THCA from the TCGA and calculated the association between PR and immune cell infiltration.

2.5.4 CIBERSORT

CIBERSORT was used to calculate the proportions of 22 human immune cell subsets with a sum of 1 (20). One thousand permutations and a p-value < 0.05 were set as the criteria for effective sample deconvolution. We compared the proportions of immune cell subsets between the L-PR and H-PR groups using the Mann-Whitney test. We performed Spearman correlation analysis between immune cells with the “corrplot” package.

2.5.5 Single-sample gene set enrichment analysis (ssGSEA)

We quantified the enrichment levels of 29 immune signatures in each THCA sample by the ssGSEA score (21). Based on the ssGSEA scores of the 29 immune signatures, we explored differences in the immune characteristics of the L-PR and H-PR groups (Table S1).

We corrected the data to facilitate presentation of the overall results. Each ssGSEA score, Xi, was transformed into Xi' with the equation $Xi'=(Xi - X_{min})/(X_{max}-X_{min})$, where X_{min} and X_{max} represent the minimum and maximum ssGSEA scores, respectively, for the immune gene set across all THCA samples.

2.5.6 TMB

THCA simple nucleotide variation data from the TCGA (VarScan) and a validated algorithm (22) were used to calculate the TMB, which was defined as the number of mutations per megabase.

2.5.7 Gene set enrichment analysis (GSEA)

GSEA software (version 2.0.1) was downloaded from the Broad Institute (http://www.broad.mit.edu/gsea). Normalized enrichment score (NES) and false discovery rate (FDR) values were used to sort the results of GSEA (KEGG pathway) of the L-PR and H-PR groups with 1000 gene set permutations for each analysis. Results for which |NES | ≥1.0, p-value ≤ 0.05, and FDR q-val ≤ 0.25 were considered statistically significant.

2.6 GEO verification

The PR for each PTC sample in the TCGA dataset was calculated using the prognostic model, and samples were divided into L-PR and H-PR groups by the median PR. ssGSEA and ESTIMATE were used to verify the immune efficacy of the PR in five GEO datasets (GSE33630, GSE60542, GSE58545, GSE5364, and GSE27155).

2.7 Statistical analysis

Kaplan-Meier (K-M) survival analysis was performed using the R package "survival" (with PFS as the ending indicator). The survival receiver operating characteristic (ROC) curve and area under the ROC (AUC) were determined with the "survival ROC" package in R. The chi-square test was used to assess differences in clinical parameters between the L-PR and H-PR groups. The Mann-Whitney U test and *t*-test were used for comparisons between the two groups. The Spearman and Pearson methods were used for correlation analysis. Significant survival p-values were calculated using the log-rank method. SPSS version 25.0 software and R software (version 3.6.0) were used to analyze the data. Data were visualized with R, GraphPad Prism version 8.0 and Excel software.

3 Results

3.1 Identification of DEGs

A total of 2696 DEGs between PTC and normal tissues, comprising 1470 upregulated and 1226 downregulated DEGs, were extracted from the TCGA (Figure S1A and B). A total of 115 upregulated and 118 downregulated DEGs were common to analyses of PTC and normal tissues in 5 GEO datasets (GSE33630, GSE60542, GSE58545, GSE3467, and GSE3678) and were used to verify the DEGs from the

TCGA dataset. A total of 113 upregulated and 105 downregulated genes were common to all 6 datasets (Figure S1C), which indicated the accuracy of gene selection.

3.2 Inflammatory manifestations in PTC

As expected, inflammatory pathways were most frequently implicated by functional enrichment analysis of PTC data. The GO terms “extracellular structure organization,” “extracellular matrix,” and “serine-type peptidase activity” were the GO biological process, cellular component, and molecular function GO terms, respectively, most enriched in the DEGs (Fig. 2A). The “cytokine-cytokine receptor interactions” pathway was the KEGG pathway most significantly enriched in the DEGs (Fig. 2B). According to ssGSEA score, the expression levels of 29 immune-associated gene sets representing diverse immune cell types, functions, and pathways tended to be increased in PTC compared to the adjacent normal tissues (Fig. 2C). In summary, PTC exhibited significant inflammatory characteristics.

3.3 Evaluation of modeling clinical outcomes

Thirteen genes were selected by LASSO during the modeling process (Fig. 3A and B and Table S2). Univariate Cox regression analysis was used to determine whether these genes are potential biomarkers and qualified to monitor prognosis (Figure S2).

Based on the results of multivariate Cox regression analysis, we constructed a prognostic signature to divide the PTC patients into two groups with discrete clinical outcomes as determined by PFS (Fig. 3C-E). The following formula was used:

PR=[expression level of *FAXDC2* * (0.01224)] + [expression level of *COL1A1* * (0.0005941)] + [expression level of *MLF1* * (0.4253)] + [expression level of *CTSC* * (0.02736)] + [expression level of *WWOX* * (0.2452)] + [expression level of *FN1* * (0.0005180)] + [expression level of *NPC2* * (-0.0002628)] + [expression level of *HBB* * (-0.007181)] + [expression level of *LYVE1* * (-0.5555)] + [expression level of *MPZL2* * (-0.02449)] + [expression level of *TENM1* * (0.04534)] + [expression level of *DUSP6* * (-0.0004503)] + [expression level of *AHNAK2* * (0.05361)].

The PR could be an important tool in distinguishing PTC patient clinical outcomes (Fig. 4A). The AUC at 3, 5, and 10 years was 0.831, 0.861, and 0.873, respectively (Fig. 4B), suggesting that the prognostic signature can be used to efficiently monitor survival. Multivariate Cox regression analysis suggested that PR is an independent predictor after other parameters (age, gender, American Joint Committee on Cancer (AJCC) stage, T classification, N classification, metastasis, radiation therapy, TMB and mutations in *BRAF* and *RAS*) are adjusted (Table 1). The prognostic signature was also found to be a viable index reflecting overall survival (OS) and relapse-free survival (RFS) in different PTC patients (Fig. 4C and D).

Table 1
Univariate and multivariate regression analysis of PTC.

Variables	Univariate analysis		Multivariate analysis	
	Hazard ratio (95%CI)	P value	Hazard ratio (95%CI)	P value
Age	1.054 (1.028 − 1.080)	< 0.001	1.044 (1.004 − 1.086)	0.031
Gender(male/female)	1.240 (0.539 − 2.854)	0.612	1.151 (0.435 − 3.043)	0.777
Stage	2.049 (1.440 − 2.915)	< 0.001	1.160 (0.595 − 2.260)	0.664
Metastasis	6.485 (2.182 − 19.28)	< 0.001	2.071 (0.428 − 10.02)	0.365
N classification	1.291 (0.597 − 2.792)	0.517	0.556 (0.197 − 1.568)	0.268
T classification	1.539 (0.995 − 2.380)	0.053	1.041 (0.562 − 1.928)	0.898
Radiation therapy	1.896 (0.797 − 4.512)	0.148	1.863 (0.607 − 5.715)	0.277
BRAF mutation	0.672 (0.307 − 1.468)	0.318	1.045 (0.342 − 3.191)	0.939
RAS mutation	1.715 (0.586 − 5.018)	0.325	1.644 (0.324 − 8.331)	0.548
TMB	5.008 (2.414 − 10.39)	< 0.001	1.611 (0.482 − 5.382)	0.439
Risk score	1.284 (1.204 − 1.369)	< 0.001	1.306 (1.179 − 1.448)	< 0.001

In summary, the PR exhibited outstanding efficacy as an independent prognostic factor.

3.4 Clinical utility of the prognostic signature

The relationships between the PR and the following clinical parameters were analyzed: age, gender, stage, T classification, N classification, metastasis, pathologic type, radiation therapy, mutation of *BRAF* and *RAS*, and vital statistics (Table 2). The PR was significantly higher in seniors; patients with advanced stage PTC, advanced T classification, distant metastasis, *RAS* mutation, and follicular and tall cell PTC.

Table 2
Comparison of clinical parameters between L-PR and H-PR groups in PTC.

Clinical parameters	Risk score		*P* value
	Low (n = 251, %)	High (n = 251, %)	
Age(y)			
< 55	195 (77.7)	140 (55.8)	< 0.001
≥ 55	56 (22.3)	111 (42.2)	
Gender			
Female	182 (72.5)	185 (73.7)	0.763
Male	69 (27.5)	66 (26.3)	
Stage			
I	165 (65.7)	116 (46.2)	< 0.001
II	18 (7.2)	34 (13.5)	
III	43 (17.1)	69 (27.5)	
IV	25 (10.0)	30 (12.0)	
NA	0	2 (0.8)	
T classification			
T1	93 (37.1)	50 (20.0)	< 0.001
T2	79 (31.5)	85 (33.9)	
T3	70 (27.9)	100 (39.8)	
T4	8 (3.2)	15 (6.0)	
NA	1 (0.4)	1 (0.4)	
N classification			
N0	115 (45.8)	114 (45.4)	0.445
N1	120 (47.8)	103 (41.0)	
NA	16 (6.4)	34 (31.5)	
Metastasis			
M0	155 (61.8)	127 (50.6)	0.009
M1	1 (0.4)	8 (3.2)	
NA	95 (37.8)	116 (46.2)	

Clinical parameters	Risk score		*P* value
	Low (n = 251, %)	High (n = 251, %)	
Radiation therapy			
No	99 (39.4)	78 (31.1)	0.056
Yes	143 (57.0)	162 (64.5)	
NA	9 (3.6)	11 (4.4)	
Pathologic type			
Classical	195 (77.7)	161 (64.1)	0.006
Follicular	42 (16.7)	59 (23.5)	
Tall Cell	11 (4.4)	25 (10.0)	
Other	3 (1.2)	6 (2.4)	
BRAF			
Wild	89 (35.5)	106 (42.2)	0.115
Mutation	152 (60.6)	135 (53.8)	
NA	10 (4.0)	10 (4.0)	
RAS			
Wild	220 (87.6)	202 (80.5)	0.013
Mutation	21 (8.4)	39 (15.5)	
NA	10 (4.0)	10 (4.0)	
Vital stats(as follow-up)			
Alive	250 (99.6)	235 (93.6)	< 0.001
Dead	0	16 (6.4)	
NA	1 (0.4)	0	

In addition, due to the lack of clinical data in the GEO dataset, we only retrieved and verified the clinical data in the GSE60542 cohort. The results also showed that the PR was positively correlated with stage, maximum primary tumor size, and maximum metastatic lymph node size (Figure S3A-D).

In summary, the PR is positively correlated with PTC progression.

3.5 Comparison of the TME compositions of the L-PR and H-PR groups

The results of ESTIMATE analysis suggested that the L-PR group had a higher immune score and stromal score, while the H-PR group had a higher tumor purity score (Fig. 5A-D). These results indicated that the group with a good prognosis had a higher proportion of immune cells and stromal cells, while the group with a poor prognosis had a higher proportion of tumor cells.

mRNAsi analysis showed that the H-PR group had higher mRNAsi levels (Fig. 5E). This finding indicated that a high PR is positively correlated with a large number of CSCs.

In summary, low immune infiltration and a large number of CSCs in the TME were highly correlated with poor prognosis in PTC.

3.6 Comparison of immune cell abundance in the L-PR and H-PR groups

We used the ssGSEA score to quantify the enrichment levels of immune cells, functions and pathways in the groups with different PRs (Fig. 6A). The expression levels of genes in the immune-associated gene sets in the L-PR group generally tended to be increased, and this difference was significant in 20 of the 29 gene sets ($p < 0.05$) (type II IFN response, Tregs, tumor-infiltrating lymphocytes (TILs), TH1 cells, follicular helper T (Tfh) cells, T helper cells, T cell costimulation, T cell coinhibition, plasmacytoid dendritic cells (pDCs), parainflammation, neutrophils, mast cells, macrophages, inflammation-promoting activity, cytolytic activity, checkpoints, CD8 + T cells, CCR, B cells, and antigen-presenting cell (APC) costimulation).

To determine whether the PR accurately reflects the status of the PTC immune microenvironment, TIMER was used to analyze the relationship between PR and immune cell infiltration (Fig. 6B-G). With the exception of CD4 + T cells, the numbers of which were no different, B cells, CD8 + T cells, neutrophils, macrophages, and DCs were significantly elevated in the L-PR group compared to the H-PR group.

Additionally, immune-related gene expression levels in the L-PR group were increased overall compared to those in the H-PR group. Expression of the immune cell marker genes (23) *CD8A* (cytotoxic T cells), *CD20* (B cells), *CXCR5* (Tfh cells), *CD68* (macrophages), *IL3RA* (pDCs), and *FOXP3* (Tregs) tended to be increased in general in the L-PR group compared to the H-PR group (Figure S4A). *HLA* genes, especially *HLA* class II genes that present exogenous antigens, exhibited increased expression levels in the L-PR group compared to the H-PR group (Figure S4B). Moreover, expression levels of classical checkpoints that suppress the immune system (*CTLA4* and *PD1*) were also increased in L-PR group compared to the H-PR group (Figure S4C).

In summary, compared to the L-PR group, the overall immune cell abundance of the H-PR group was decreased.

3.7 Comparison of immune cell proportions in the L-PR and H-PR groups

CIBERSORT was used to calculate the proportion of each of the 22 immune cell types, which were compared between the L-PR and H-PR groups (Fig. 7A-C). The L-PR group exhibited higher proportions of antitumor immune cells (B cells, CD8 + T cells, M1 macrophages, and γδ T cells), while the H-PR group exhibited higher proportions of tumor-promoting immune cells (Tregs, monocytes, and activated dendritic cells (aDCs)). Additionally, positive correlations between antitumor immune cells (plasma cells, CD8 + T cells, M1 macrophages, and Tfh cells) were observed (Fig. 7D). In addition, these tumor-antagonizing immune cells were negatively correlated with immune cells with tumor-promoting effects (M2 macrophages, M0 macrophages, aDCs, resting mast cells, and resting memory CD4 + T cells) (Fig. 7D). To facilitate the understanding of these results, we listed the results in a balance chart (Fig. 7E). The balance chart was constructed based on reviews by Varricchi et al. (9) Galdiero et al. (10) and Ferrari et al. (11).

In summary, compared to the L-PR group, the H-PR group had a higher proportion of tumor-promoting immune cells and a lower proportion of antitumor immune cells.

3.8 Correlation between the TMB and the PR or PTC prognosis

We calculated the PTC TMB to reveal the top ten most frequently mutated genes in PTC (Fig. 8A). Then, we divided the 487 cases in the TCGA dataset into high-TMB and low-TMB groups based on the median TMB value. K-M survival analysis indicated that a high TMB is associated with a worse prognosis (log-rank p-value = 0.022) (Fig. 8B). Our results showed that TMB levels were significantly higher in the H-PR group (Fig. 8C). In addition, we also found that PTC samples with mutations (BRAF, RET and RAS) in the GSE60542 verification cohort had a higher PR (Figure S5).

These results indicate that the PR and TMB are positively correlated, and the TMB is negatively correlated with prognosis.

3.9 GSEA of the L-PR and H-PR groups

To understand the mechanism of PTC prognosis and functional differences between the L-PR and H-PR groups, GSEA was used to identify KEGG pathways enriched in each group. Interestingly, citrate cycle (TCA cycle); propanoate metabolism; valine, leucine and isoleucine degradation; pyruvate metabolism; aminoacyl tRNA biosynthesis, arginine and proline metabolism; nicotinate and nicotinamide metabolism; glycolysis gluconeogenesis; lysine degradation; tryptophan metabolism; and fatty acid metabolism pathways were enriched in the H-PR group (Fig. 9A). This suggests that a high PR is associated with dysregulated energy metabolism. In contrast, immune-related pathways were highly enriched in the L-PR group (Fig. 9B); these pathways included the cytokine-cytokine receptor interaction, JAK-STAT signaling, B cell receptor signaling, NK cell-mediated cytotoxicity, Toll-like receptor signaling, T cell receptor signaling, leukocyte transendothelial migration, complement and coagulation cascade pathways. This finding confirmed that the L-PR group had higher immunological activity. In addition, we identified a number of cancer-associated pathways enriched in the L-PR group; these pathways included the TC, ErbB

signaling, Notch signaling, and colorectal cancer pathways, which suggests that the activity of these cancer-related pathways is related to PR (Table S3). In general, immune-related pathways and some cancer-related pathways were enriched in the L-PR group, while metabolic pathways were enriched in the H-PR group.

3.10 GEO verification of immune characteristics of the L-PR and H-PR groups

Five GEO validation cohorts (GSE33630, GSE60542, GSE58545, GSE5364, and GSE27155) were used to verify the immune value of the PR (Fig. 10A-Y). The PR for each PTC sample in the TCGA dataset was calculated with the established model, and samples were also divided into L-PR and H-PR groups by the median PR. Through ssGSEA, we confirmed that genes involved in immune-related functions and pathways were more highly expressed in the L-PR group. In addition, through ESTIMATE, we also verified that the PR was negatively correlated with the immune score and stromal score and positively correlated with tumor purity. In summary, we confirmed the negative correlation between PR and immune infiltration.

4 Discussion

In this study, we established a scoring model (PR) that can effectively predict prognosis and explored the potential relationship between prognosis and the TME. The H-PR group, which had poor prognostic features, showed four main characteristics: 1. comprehensive weakening of the immune system, 2. an increased ratio of tumor-promoting immune cells, 3. an increased number of CSCs, and 4. an increased TMB (Fig. 11).

The importance of the TME in tumor progression and immunotherapy has been recognized. TC is an inflammation-driven cancer (8, 24, 25). Our research confirmed the enrichment of inflammatory features in PTC, which was our initial clue to examine the TME. In recent years, remarkable progress has been made in the characterization of several immune cell types (but not all) in the TME of different TCs (9, 24–34). In different stages of PTC, tumor-promoting and antitumor immune cells engage in confrontation. However, many aspects of the immune-related molecular mechanisms of PTC remain unclear, and the relationship between immune cells and prognosis has yet to be discovered. Our research provides adequate data for such an assessment. Studies have reported differences in the TME between PTC and nontumor samples, but no systematic study to explore the characteristics of the TME and progression in PTC has been carried out. We have conducted a series of studies on the above issues and obtained abundant interpretive results.

To develop a simple and convenient signature with which to monitor the immune status of PTC patients and suggest clinical outcomes, we created a prognostic model based on 13 VDEGs. Due to the excellent prognosis of PTC, the number of OS and DFS events in PTC are small, and metastasis and recurrence have become the main in its clinical management. Therefore, we chose PFS as the ending indicator. In recent years, models that predict the prognosis of PTC have developed rapidly. The 35 gene-based

prognostic scoring system developed by Pak et al. (35) shows strong discriminatory power in the prediction of event-free survival. Lin et al. (36) used DEGs to develop a risk index model to predict the prognosis of PTC. Liu et al. (37) established a prognostic model based on two microRNAs. You et al. (38) defined a signature to predict the prognosis of PTC consisting of three long noncoding RNAs (lncRNAs). A competing endogenous RNA (ceRNA) network for the prediction of tumor recurrence has also been reported (39). Our study was performed not only to establish an accurate and reliable prognostic model, but also to compare the differences between prognostic groups and to explore the potential mechanisms that cause differences in PTC prognoses.

By ESTIMATE analysis, we found that a high PR indicated a lower degree of immune cell and stromal cell infiltration and a higher tumor purity, and these samples showed that overall immune infiltration was decreased in the poor prognosis group. ssGSEA and TIMER analysis confirmed an overall decrease in immune cell abundance in the H-PR group. Moreover, the comprehensive increase in immune-related gene expression levels in the L-PR group confirmed a highly active immune system (with both tumor-antagonizing and tumor-promoting effects) in the group with a good prognosis. This finding is different from the general conclusion of previous TC studies that anticancer immune cells are positively correlated with prognosis, while cancer-promoting immune cells are negatively correlated with prognosis (34, 40–47). Our previous research also found that the immune system as a whole has a high degree of consistency in the occurrence and development of PTC. Immune escape as a tumor hallmark has been shown to be associated with poor prognosis in a variety of tumors (48, 49). The immune editing hypothesis was proposed by Dunn et al. (50) and divided the interaction between the immune system and the tumor into three stages: 1. elimination, in which immune effector cells (NK cells, CTLs and γδ T cells) recognize and destroy transformed tumor cells; this stage is also called immune surveillance; 2. equilibrium, in which the immune system eliminates tumor cells with high immunogenicity, while tumor cells with low immunogenicity survive; and 3. escape, in which tumor cells eventually escape the body's immune surveillance. The entire process results in decreased tumor immunity (51). In our study, the L-PR group showed the characteristics of the "elimination" stage, while the H-PR group showed more characteristics of the "escape" stage. Poschke et al. (52) suggested that tumors have two methods of immune escape: camouflage and sabotage. Camouflage refers to the malformation and loss of the major histocompatibility complex class I (MHC-I) molecules on the surfaces of tumors, allowing tumors to escape the detection of the immune system. The MHC in humans is also called *HLA*, and our results showed that *HLA* gene expression was lower in the H-PR group than in the L-PR group. Sabotage refers to the ability of some tumors, including PTC, to manipulate part of the immune system to fight against the body's immune response to protect themselves. In this process, tumors attract and even mediate some immune cells, such as TAMs, MDSCs, Tregs, and mast cells (MCs). In general, MDSCs, Tregs, and MCs respond to uncontrolled inflammatory reactions in the body, but during tumor progression, they create an immune microenvironment that allows this process.

Existing evidence shows that B cells, CD8 + T cells, M1 macrophages, TH1 cells, NK cells, mDCs, and γδ T cells have tumor-antagonizing effects in the PTC TME, while Tregs, TH2 cells, M2 macrophages, MDSCs, iDCs, mast cells, monocytes, and neutrophils have tumor-promoting effects (9–11). Our previous research

also showed that during the occurrence and development of PTC, the proportion of tumor-promoting immune cells (M2 macrophages, Tregs, monocytes, neutrophils, DCs, MCs, and M0 macrophages) increased, while the proportion of antitumor immune cells (M1 macrophages, CD8 + T cells, B cells, NK cells, Tfh cells, and γδ T cells) decreased (53). In this study, the H-PR group showed a high proportion of tumor-promoting immune cells (Tregs, monocytes and aDCs) and a lower proportion of antitumor immune cells (B cells, CD8 + T cells, M1 macrophages and γδ T cells), indicating that the tumor cells escaped the body's immune surveillance by "sabotage" and achieved immune escape. Based on the above conclusions, we speculate that the irreversible progression of tumors caused by immune escape in the PTC TME is a crucial cause of poor prognosis. The enrichment of immune-related pathways in the L-PR group by GSEA also supports the above view.

Tumor heterogeneity, one of the characteristics of malignant tumors, can cause differences in tumor growth rate, invasion and prognosis. Two models have been used to explain the heterogeneity of cancer cells (54). The first is the stochastic model, in which the development of cancer is triggered by the accumulation of gene mutations in a single cancer cell, followed by different subsequent genetic events in different subpopulations of cells. We found that the H-PR group had a significantly higher TMB than the L-PR group. In 2019, the TMB was included in the NCCN index as an emerging prognostic indicator in non-small cell lung cancer immunotherapy (12–15, 55). We found that PTC patients with a high TMB had a worse prognosis. Other studies have also reported that patients with a variety of cancer types with a high TMB can obtain a better prognosis after immunotherapy; however, without immunotherapy, patients with a high TMB show a poor prognosis (56). Our study fills the gap in knowledge of the role of TMB in PTC. The high TMB observed in patients with a poor prognosis suggests immunotherapy as a viable option for these patients.

The second model is the CSC model, which postulates that a small population of cells in the tumor is responsible for tumor initiation, growth, and recurrence (57). We found that the H-PR group had a higher CSC content than the L-PR group. The positive correlation between CSCs and recurrence and metastasis in our data can be explained well by the CSC model (6). CSCs in cancer biology are resistant to conventional therapies (such as surgery and radioactive iodine therapy), and TC usually relapses as CSCs recur (58). The combination of CSC-specific therapies (such as drugs that target the Notch or MEK and JNK pathways as therapeutics to eliminate CSCs) with conventional therapies has the potential to eradicate highly lethal cancers (58).

In addition, PTCs with high tumor heterogeneity have a higher frequency of weak immunogenic tumor cells, which will also accelerate the body's immune selection for tumor cells and exacerbate immune escape (59).

At present, PTC immunotherapy is an active research field, and the study of the tumor immune microenvironment is an important pillar of research on PTC management via immunotherapy (4). The results of this study provide a reference for subsequent research on the PTC immune microenvironment. The high level of immune escape and high TMB shown by the H-PR group suggest that immunotherapy

is a viable option for patients with poor prognosis. The PR as a prognostic signature and an immune status indicator can assist in the clinical stratification of PTC patients to identify patients who respond to immunotherapy.

However, this study has some limitations. 1. Because the TCGA is the only public database with sufficient data on both PTC expression and prognosis, we did not use other independent cohorts to verify the prognostic value of the PR. However, we confirmed the negative correlation between the PR and immune infiltration in 5 GEO verification cohorts and verified the positive correlation between the PR and PTC progression and mutation in GSE60542 using clinical data. 2. The PR has a strong predictive effect on PTC prognosis, but there may still be slight differences in the TME between the PR grouping method and the actual different prognosis grouping method. However, related prognostic research is ongoing. 3. Cancer-related pathway enrichment in the L-PR group has not been well explained, but we suspect that this enrichment is related to increased immune infiltration. It was also found in triple-negative breast cancers that a group with a high level of immune infiltration showed a better prognosis, accompanied by the enrichment of cancer-related pathways (60).

5 Conclusions

In summary, we have established a prognostic model that can effectively predict the prognosis of PTC and revealed that immune escape and tumor heterogeneity in the TME could be mechanisms of poor prognosis in PTC.

Declarations

Ethics approval and consent to participate

Not applicable.

Availability of data and materials

A thyroid carcinoma (THCA) dataset from The Cancer Genome Atlas (TCGA) with 58 normal thyroid samples (N) and 512 PTC samples (T) was selected as the discovery cohort. Normalized level-three RNA-seq fragments per kilobase of exon per million fragments mapped (FPKM) data and simple nucleotide variation data (VarScan) were downloaded from the TCGA Genomics Data Commons (GDC) (https://portal.gdc.cancer.gov/). Clinical THCA TCGA data were downloaded from the University of California at Santa Cruz (UCSC) Xena platform (https://xena.ucsc.edu/).

The abovementioned 7 PTC gene expression microarray datasets were downloaded from the National Center for Biotechnology Information Gene Expression Omnibus (GEO) database (http://www.ncbi.nlm.nih.gov/geo): GSE33630 (N=45, T=49), GSE60542 (N=30, T=33), GSE58545 (N=18, T=27), GSE3467 (N=9, T=9), GSE3678 (N=7, T=7), GSE5364 (T=35), and GSE27155 (T=51).

Competing interests

The authors have declared that no competing interest exists.

Authors' contributions

Xinyang Li designed the analytical strategies, performed data analyses and wrote the manuscript. Zhenyu Xie,Yinde Huang,Xin Li,Yuzhen He,Song Wu,Shiyue Wang,Wenbin Chen and Yuchen He performed data analyses. Jian Zhang conceived the research and wrote the manuscript.

Funding

This research was supported by the National Natural Science Foundation of China (81600602).

Acknowledgments

We would like to thank Mr. Guangqi Li for his support with bioinformatics analysis and pay tribute to the contributions of public databases such as the TCGA and GEO to human medicine.

References

1. Lim H, Devesa SS, Sosa JA, Check D, Kitahara CM. Trends in Thyroid Cancer Incidence and Mortality in the United States, 1974–2013. JAMA. 2017;317:1338–48.
2. Cabanillas ME, McFadden DG, Durante C. Thyroid cancer. Lancet. 2016;388:2783–95.
3. Fagin JA, Wells SA. Biologic and clinical perspectives on thyroid cancer. N Engl J Med. 2016;375:1054–67.
4. Naoum GE, Morkos M, Kim B, Arafat W. Novel targeted therapies and immunotherapy for advanced thyroid cancers. Mol Cancer. 2018;17:51.
5. Brito JP, Hay ID, Morris JC. Low risk papillary thyroid cancer. BMJ. 2014;348:g3045.
6. Hanahan D, Weinberg RA. Hallmarks of cancer: the next generation. Cell. 2011;144:646–74.
7. Rotondi M, Coperchini F, Latrofa F, Chiovato L. Role of chemokines in thyroid cancer microenvironment: is CXCL8 the main player? Front Endocrinol (Lausanne). 2018;9:314.
8. Thorsson V, Gibbs DL, Brown SD, Wolf D, Bortone DS, Ou Yang TH, et al. The immune landscape of cancer. Immunity. 2018; 48:812 – 30.e14.
9. Varricchi G, Loffredo S, Marone G, Modestino L, Fallahi P, Ferrari SM, et al. The immune landscape of thyroid cancer in the context of immune checkpoint inhibition. Int J Mol Sci. 2019;20:3934.
10. Galdiero MR, Varricchi G, Marone G. The immune network in thyroid cancer. Oncoimmunology. 2016;5:e1168556.
11. Ferrari SM, Fallahi P, Galdiero MR, Ruffilli I, Elia G, Ragusa F, et al. Immune and inflammatory cells in thyroid cancer microenvironment. Int J Mol Sci. 2019;20:4413.

12. Carbone DP, Reck M, Paz-Ares L, Creelan B, Horn L, Steins M, et al. First-line nivolumab in stage IV or recurrent non-small-cell lung cancer. N Engl J Med. 2017;376:2415–26.
13. Hellmann MD, Ciuleanu TE, Pluzanski A, Lee JS, Otterson GA, Audigier-Valette C, et al. Nivolumab plus ipilimumab in lung cancer with a high tumor mutational burden. N Engl J Med. 2018;378:2093–104.
14. Snyder A, Makarov V, Merghoub T, Yuan J, Zaretsky JM, Desrichard A, et al. Genetic basis for clinical response to CTLA-4 blockade in melanoma. N Engl J Med. 2014;371:2189–99.
15. Yarchoan M, Hopkins A, Jaffee EM. Tumor mutational burden and response rate to PD-1 inhibition. N Engl J Med. 2017;377:2500–1.
16. Jiang Y, Zhang Q, Hu Y, Li T, Yu J, Zhao L, et al. ImmunoScore signature: a prognostic and predictive tool in gastric cancer. Ann Surg. 2018;267:504–13.
17. Yoshihara K, Shahmoradgoli M, Martinez E, Vegesna R, Kim H, Torres-Garcia W, et al. Inferring tumour purity and stromal and immune cell admixture from expression data. Nat Commun. 2013;4:2612.
18. Malta TM, Sokolov A, Gentles AJ, Burzykowski T, Poisson L, Weinstein JN, et al. Machine learning identifies stemness features associated with oncogenic dedifferentiation. Cell. 2018; 173:338 – 54.e15.
19. Li T, Fan J, Wang B, Traugh N, Chen Q, Liu JS, et al. TIMER: a web server for comprehensive analysis of tumor-infiltrating immune cells. Cancer Res. 2017;77:e108-10.
20. Newman AM, Liu CL, Green MR, Gentles AJ, Feng W, Xu Y, et al. Robust enumeration of cell subsets from tissue expression profiles. Nat Methods. 2015;12:453–7.
21. Barbie DA, Tamayo P, Boehm JS, Kim SY, Moody SE, Dunn IF, et al. Systematic RNA interference reveals that oncogenic KRAS-driven cancers require TBK1. Nature. 2009;462:108–12.
22. Chalmers ZR, Connelly CF, Fabrizio D, Gay L, Ali SM, Ennis R, et al. Analysis of 100,000 human cancer genomes reveals the landscape of tumor mutational burden. Genome Med. 2017;9:34.
23. Bindea G, Mlecnik B, Tosolini M, Kirilovsky A, Waldner M, Obenauf AC, et al. Spatiotemporal dynamics of intratumoral immune cells reveal the immune landscape in human cancer. Immunity. 2013;39:782–95.
24. Cunha LL, Marcello MA, Ward LS. The role of the inflammatory microenvironment in thyroid carcinogenesis. Endocr Relat Cancer. 2014;21:R85–103.
25. Fridman WH, Zitvogel L, Sautès-Fridman C, Kroemer G. The immune contexture in cancer prognosis and treatment. Nat Rev Clin Oncol. 2017;14:717–34.
26. Matsubayashi S, Kawai K, Matsumoto Y, Mukuta T, Morita T, Hirai K, et al. The correlation between papillary thyroid carcinoma and lymphocytic infiltration in the thyroid gland. J Clin Endocrinol Metab. 1995;80:3421–4.
27. Kim S, Cho SW, Min HS, Kim KM, Yeom GJ, Kim EY, et al. The expression of tumor-associated macrophages in papillary thyroid carcinoma. Endocrinol Metab (Seoul). 2013;28:192–8.

28. French JD, Weber ZJ, Fretwell DL, Said S, Klopper JP, Haugen BR. Tumor-associated lymphocytes and increased FoxP3 + regulatory T cell frequency correlate with more aggressive papillary thyroid cancer. J Clin Endocrinol Metab. 2010;95:2325–33.
29. Visciano C, Liotti F, Prevete N, Cali G, Franco R, Collina F, et al. Mast cells induce epithelial-to-mesenchymal transition and stem cell features in human thyroid cancer cells through an IL-8-Akt-Slug pathway. Oncogene. 2015;34:5175–86.
30. Gupta S, Patel A, Folstad A, Fenton C, Dinauer CA, Tuttle RM, et al. Infiltration of differentiated thyroid carcinoma by proliferating lymphocytes is associated with improved disease-free survival for children and young adults. J Clin Endocrinol Metab. 2001;86:1346–54.
31. Ryder M, Ghossein RA, Ricarte-Filho JC, Knauf JA, Fagin JA. Increased density of tumor-associated macrophages is associated with decreased survival in advanced thyroid cancer. Endocr Relat Cancer. 2008;15:1069–74.
32. Gogali F, Paterakis G, Rassidakis GZ, Kaltsas G, Liakou CI, Gousis P, et al. Phenotypical analysis of lymphocytes with suppressive and regulatory properties (Tregs) and NK cells in the papillary carcinoma of thyroid. J Clin Endocrinol Metab. 2012;97:1474–82.
33. Gogali F, Paterakis G, Rassidakis GZ, Liakou CI, Liapi C. CD3(-)CD16(-)CD56(bright) immunoregulatory NK cells are increased in the tumor microenvironment and inversely correlate with advanced stages in patients with papillary thyroid cancer. Thyroid. 2013;23:1561–8.
34. Cunha LL, Morari EC, Guihen AC, Razolli D, Gerhard R, Nonogaki S, et al. Infiltration of a mixture of immune cells may be related to good prognosis in patients with differentiated thyroid carcinoma. Clin Endocrinol (Oxf). 2012;77:918–25.
35. Pak K, Kim YH, Suh S, Goh TS, Jeong DC, Kim SJ, et al. Development of a risk scoring system for patients with papillary thyroid cancer. J Cell Mol Med. 2019;23:3010–5.
36. Lin P, Guo YN, Shi L, Li XJ, Yang H, He Y, et al. Development of a prognostic index based on an immunogenomic landscape analysis of papillary thyroid cancer. Aging. 2019;11:480–500.
37. Liu T, You X, Sui J, Shen B, Zhang Y, Zhang XM, et al. Prognostic value of a two-microRNA signature for papillary thyroid cancer and a bioinformatic analysis of their possible functions. J Cell Biochem. 2018. doi:10.1002/jcb.27993.
38. You X, Yang S, Sui J, Wu W, Liu T, Xu S, et al. Molecular characterization of papillary thyroid carcinoma: a potential three-lncRNA prognostic signature. Cancer Manag Res. 2018;10:4297–310.
39. Chen F, Li Z, Deng C, Yan H. Integrated analysis identifying new lncRNA markers revealed in ceRNA network for tumor recurrence in papillary thyroid carcinoma and build of nomogram. J Cell Biochem. 2019;120:19673–83.
40. Jung KY, Cho SW, Kim YA, Kim D, Oh BC, Park DJ, et al. Cancers with higher density of tumor-associated macrophages were associated with poor survival rates. J Pathol Transl Med. 2015;49:318–24.
41. Liu CL, Lee JJ, Liu TP, Chang YC, Hsu YC, Cheng SP. Blood neutrophil-to-lymphocyte ratio correlates with tumor size in patients with differentiated thyroid cancer. J Surg Oncol. 2013;107:493–7.

42. Lee F, Yang PS, Chien MN, Lee JJ, Leung CH, Cheng SP. An increased neutrophil-to-lymphocyte ratio predicts incomplete response to therapy in differentiated thyroid cancer. Int J Med Sci. 2018;15:1757–63.
43. Lee KH, Seok EY, Kim EY, Yun JS, Park YL, Park CH. Different prognostic values of individual hematologic parameters in papillary thyroid cancer due to age-related changes in immunity. Ann Surg Treat Res. 2019;96:70–7.
44. Ozmen S, Timur O, Calik I, Altinkaynak K, Simsek E, Gozcu H, et al. Neutrophil-lymphocyte ratio (NLR) and platelet-lymphocyte ratio (PLR) may be superior to C-reactive protein (CRP) for predicting the occurrence of differentiated thyroid cancer. Endocr Regul. 2017;51:131–6.
45. Aghajani MJ, Yang T, McCafferty CE, Graham S, Wu X, Niles N. Predictive relevance of programmed cell death protein 1 and tumor-infiltrating lymphocyte expression in papillary thyroid cancer. Surgery. 2018;163:130–6.
46. Hilly O, Rath-Wolfson L, Koren R, Mizrachi A, Hamzany Y, Bachar G, et al. CD1a-positive dendritic cell density predicts disease-free survival in papillary thyroid carcinoma. Pathol Res Pract. 2015;211:652–6.
47. Pilli T, Toti P, Occhini R, Castagna MG, Cantara S, Caselli M, et al. Chronic lymphocytic thyroiditis (CLT) has a positive prognostic value in papillary thyroid cancer (PTC) patients: the potential key role of Foxp3 + T lymphocytes. J Endocrinol Invest. 2018;41:703–9.
48. Mittal D, Gubin MM, Schreiber RD, Smyth MJ. New insights into cancer immunoediting and its three component phases–elimination, equilibrium and escape. Curr Opin Immunol. 2014;27:16–25.
49. Rosenthal R, Cadieux EL, Salgado R, Bakir MA, Moore DA, Hiley CT, et al. Neoantigen-directed immune escape in lung cancer evolution. Nature. 2019;567:479–85.
50. Dunn GP, Bruce AT, Ikeda H, Old LJ, Schreiber RD. Cancer immunoediting: from immunosurveillance to tumor escape. Nat Immunol. 2002;3:991–8.
51. Kim R, Emi M, Tanabe K. Cancer immunoediting from immune surveillance to immune escape. Immunology. 2007;121:1–14.
52. Poschke I, Mougiakakos D, Kiessling R. Camouflage and sabotage: tumor escape from the immune system. Cancer Immunol Immunother. 2011;60:1161–71.
53. Xie Z, Li X, He Y, Wu S, Wang S, Sun J, et al. Immune Cell Confrontation in the Papillary Thyroid Carcinoma Microenvironment. Front Endocrinol. 2020;11:570604.
54. Nagayama Y, Shimamura M, Mitsutake N. Cancer Stem Cells in the Thyroid. Front Endocrinol (Lausanne). 2016;7:20.
55. Hellmann MD, Nathanson T, Rizvi H, Creelan BC, Sanchez-Vega F, Ahuja A, et al. Genomic features of response to combination immunotherapy in patients with advanced non-small-cell lung cancer. Cancer Cell. 2018; 33:843 – 52.e4.
56. Wang X, Li M. Correlate tumor mutation burden with immune signatures in human cancers. BMC Immunol. 2019;20:4.

57. Reya T, Morrison SJ, Clarke MF, Weissman IL. Stem cells, cancer, and cancer stem cells. Nature. 2001;414:105–11.
58. Guo Z, Hardin H, Lloyd RV. Cancer stem-like cells and thyroid cancer. Endocr Relat Cancer. 2014;21:T285–300.
59. Caswell DR, Swanton C. The role of tumour heterogeneity and clonal cooperativity in metastasis, immune evasion and clinical outcome. BMC Med. 2017;15:133.
60. He Y, Jiang Z, Chen C, Wang X. Classification of triple-negative breast cancers based on Immunogenomic profiling. J Exp Clin Cancer Res. 2018;37:327.

Supplementary Materials

The Supplementary Figures and Tables are not available with this version

Figures

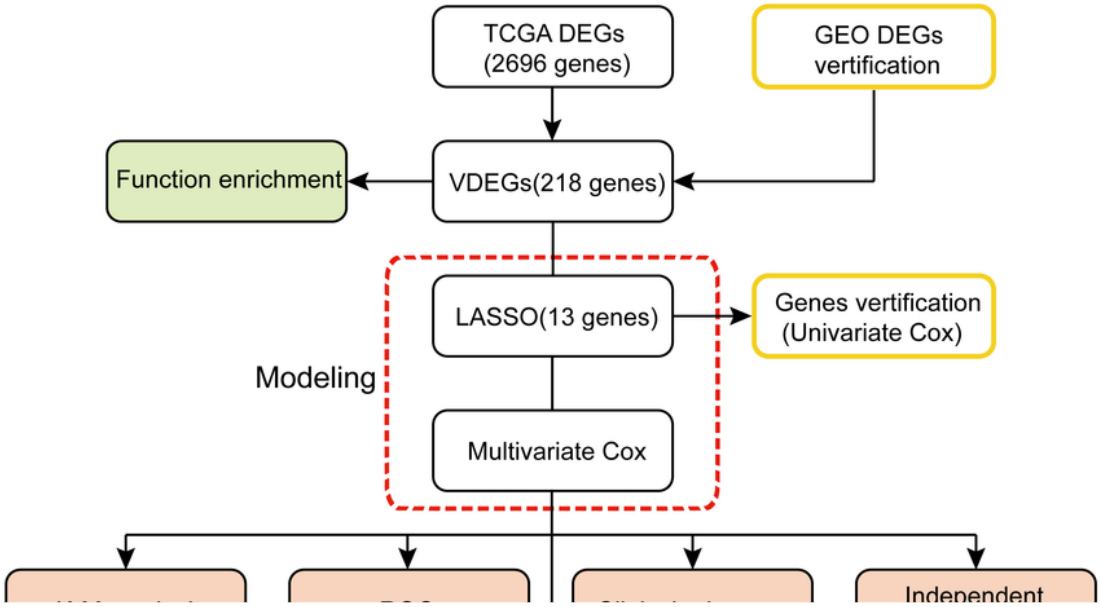

Figure 1

Main flow chart. A PTC prognostic model was established based on VDEGs, and its predictive efficacy and clinical characteristics were analyzed. Then, a series of experiments to explain prognostic differences based on the immune microenvironment were carried out. Finally, the results were verified in multiple datasets. ESTIMATE was used to evaluate the immune score, stromal score, and tumor purity in the PTC TME. The mRNAsi was used to evaluate the CSC content in the PTC TME. ssGSEA andTIMER were used

to calculate the immune cell abundance of PTC samples. CIBERSORT was used to calculate the immune cell proportions of PTC samples. GSEA was used to analyze the enrichment pathways related to PTC prognosis.

Figure 2

Functional enrichment in DEGs and inflammatory differences between PTC and normal tissues. (**A**) GO analysis; the blue, red and green areas represent biological processes, cellular components and molecular functions, respectively; (**B**) The top 9 most significantly enriched KEGG pathways; (**C**) ssGSEA of the 29 immune signatures. *p<0.05, ** p<0.01, *** p<0.001, **** p<0.0001 here and in the following figures.

Figure 3

Establishment of a prognostic model. (**A**) In the LASSO model, 1000-fold cross-validation was used for tuning parameter selection (λ as a tuning parameter to plot partial likelihood deviance); (**B**) LASSO coefficient profiles of 218 VDEGs. The dotted line indicates the value after 1000 cross-validations. In (**A**) and (**B**), the number above the figure indicates the number of genes subjected to LASSO analysis; (**C**) A total of 502 PTC cases were divided into low prognostic risk score (L-PR) and high prognostic risk score (H-PR) groups according to the median PR; (**D**) Survival status of patients with PTC; (**E**) Heatmap showing the expression of 13 modeling genes.

Figure 4

The prognostic value of the prognostic model. (**A**) The H-PR group showed a shorter PFS time; (**B**) ROC curve validation of the predictive performance of the prognostic model. Survival analysis with an ending indicator of (**C**) OS or (**D**) RFS in PTC.

Figure 5

Relationship between PR and the tumor microenvironment in PTC. The H-PR group exhibited (**A**) lower stromal scores; (**B**) lower immune scores; (**C**) lower ESTIMATE scores; (**D**) a higher tumor purity, and (**E**) more cancer stem cells (CSCs) than the L-PR group. Stromal score, immune score, ESTIMATE score and tumor purity were evaluated by ESTIMATE. CSC levels were evaluated by expression-based stemness index (mRNAsi).

Figure 6

Comparison of immune cell infiltration (abundance) between the L-PR and H-PR groups. (**A**) Immune-related cells, functions, and pathways were comprehensively enriched in the H-PR group, as shown by ssGSEA; (**B**) B cells; (**C**) CD4+ T cells; (**D**) CD8+ T cells; (**E**) DCs; (**F**) macrophages, and (**G**) neutrophils. The abundance of the immune cell types from B to F was evaluated with the TIMER database. The Spearman method was used for correlation analysis.

Figure 7

Comparison of immune cell infiltration (proportion) between the L-PR and H-PR groups. Proportions of 22 types of immune cells (CIBERSORT) in (**A**) the L-PR group and (**B**) the H-PR group; (**C**) Comparison of immune cell proportions between the L-PR and H-PR groups. (**D**) Correlation analysis between immune cell types in PTC; (**E**) Balance chart of the differences in immune cell infiltration between the L-PR and H-PR groups.

Figure 8

The relationship of tumor mutation burden (TMB) to prognosis and the PR in PTC. Number of gene mutations and the top 30 most significantly mutated genes in (**A**) L-PR group and (**B**) H-PR group; (**C**) The high-TMB group showed a worse prognosis than the low-TMB group; (**D**) The H-PR group showed a higher TMB than the L-PR group.

Figure 9

Gene set enrichment analysis (GSEA) of PRs in PTC. (**A**) KEGG pathways enriched in the H-PR group; (**B**) KEGG pathways enriched in the L-PR group.

Figure 10

Verification of the immune value of the PR. (**A-E**) ssGSEA of the 29 immune signatures; (**F, J, N, R and V**) Differences in the stromal scores; (**G, K, O, S, and W**) immune scores; (**H, I, P, T, and X**) ESTIMATE scores, and (**I, M, Q, U, and Y**) tumor purity between the L-PR and H-PR groups were assessed. Validation cohorts

were from the GSE5364 (**A, F, G, H, and I**), GSE27155 (**B, J, K, I, and M**), GSE33630 (**C, N, O, P, and Q**), GSE58545 (**D, R, S, T, and U**), and GSE60542 (**E, V, W, X, and Y**) datasets.

Figure 11

Model diagram. PTC patients divided into two groups based on PR had different immune microenvironment characteristics and prognoses.